

Source Model of the 1995 Hyogo-ken Nanbu Earthquake and Simulation of Near-Source Ground Motion

by Katsuhiko Kamae and Kojiro Irikura

Abstract The 1995 Hyogo-Ken Nanbu earthquake struck the heavily populated Kobe and adjacent cities in western Japan. More than 6400 people were killed, and more than 150,000 buildings were destroyed. The characteristics of mainshock ground motions in the heavily damaged area are needed to understand how buildings and bridges performed and why they reached failure. Unfortunately, very few strong ground motions were recorded in the heavily damaged area during the mainshock. In this study, we attempt to estimate mainshock ground motions by using the empirical Green's function method (EGF method). First, we assume an initial source model with the asperities based on the rupture process obtained by inversion of strong-ground-motion records. For simplicity, we consider each asperity as a subevent with uniform stress drop in a finite extent. Then, the initial model was improved by matching the synthetic and observed ground motions using a trial-and-error procedure. The final model consists of three subevents: subevent 1 with stress drop of 163 bars, under the Akashi Strait around the rupture starting point; subevent 2 with stress drop of 86 bars, under the Nojima Fault in Awaji Island; and subevent 3 with stress drop of 86 bars, under Kobe. Finally, we estimate strong ground motions using aftershock records at sites where the mainshock was not recorded. The near-source motions in Kobe synthesized with the best-fit model are characterized by two large pulses with a duration of 1 to 3 sec. The pulses are caused by forward rupture directivity effects from subevents 1 and 3. Peak horizontal acceleration and velocity of the synthesized motions at the heavily damaged sites are about 1000 cm/sec^2 and 130 cm/sec , respectively, while those at a rock site in the near-source region are about 300 cm/sec^2 and 60 cm/sec .

Introduction

The 17 January 1995 Hyogo-ken Nanbu earthquake ($M_w = 6.9$) occurred just beneath Kobe, a megacity with a population of about 3 million, and caused the greatest earthquake damage in Japan since the 1923 Kanto earthquake. It is one of the most important subjects to clarify the source process in order to understand how the mainshock ground motions were generated and why they caused such severe damage. Various explanations related to the generation of destructive ground motions have already been reported. Some geologists suggested that the fault rupture ran just beneath the narrow heavily damaged area, even though there were few aftershocks located in this region (e.g., Shimamoto, 1995; Watanabe and Suzuki, 1995). By examining particle motions at strong-motion observation sites in the near-source area, Irikura (1995) has pointed out that the causative faults run along the southern edges of the known active faults and not beneath the narrow damage area. Many seismologists believe that significant amplification due to the basin-edge effect and local site effects as well as forward

source directivity are the cause of the concentration of heavy damage along a narrow zone (e.g., Kawase, 1996; Pitarka *et al.*, 1998; Koketsu, 1997).

In order to discuss how buildings and bridges performed during the earthquake and why they failed, we need to know the main characteristics of the strong ground motion. Unfortunately, very few strong ground motions were recorded in the heavily damaged areas during the mainshock. Pitarka *et al.* (1998) simulated the near-source ground motions by a purely deterministic approach based on the inverted source model. They successfully explained the appearance of the heavily damaged belt, since ground motions were amplified in a narrow zone in the sediment side due to the basin-edge effects as well as the forward rupture directivity. However, the amplitude of the synthesized motions are considerably small compared with the observed ones, because surface soft layers are not taken into account.

In this study, we attempt to estimate ground motion at the sites inside the damaged area in Kobe city using after-

shock records as empirical Green's functions. The advantage of the empirical Green's function method (EGF method) is that it includes the propagation path and local site effects and estimates basically broadband motions as long as the aftershock records are accurate enough in broad-frequency band. Aftershock observations were carried out immediately after the mainshock by a group from the Disaster Prevention Research Institute, Kyoto University, and Izumi Research Institute, Shimizu Corporation. Several sites were installed in and around the heavily damaged area in Kobe (Iwata *et al.*, 1995).

To apply the EGF method to simulate strong ground motion from the mainshock, we need a source model that is appropriate over a broad-frequency band of engineering interest (e.g., 0.1 to 20 Hz). Soon after the earthquake, Kikuchi (1995) proposed a source model consisting of three subevents by inverting teleseismic body waveforms. His result is not useful for estimating near-source ground motions because the rupture zone is not precisely located and the wavelengths used for the analysis are too long (about 100 km). In addition, the rupture process of this earthquake was determined by the inversion of the strong-ground-motion records (e.g., Sekiguchi *et al.*, 1996; Ide and Takeo, 1996) and also from the joint inversion of strong ground motion, teleseismic, and geodetic data (Horikawa, 1996; Wald, 1996; Yoshida *et al.*, 1996). However, these models are also not useful for estimating high-frequency strong ground motions because they were derived from low-pass filtered (<1.0 Hz) velocity or displacement data. On the other hand, Kakehi *et al.* (1996) estimated the radiation process of high-frequency seismic waves between 2 and 10 Hz by using the envelope inversion of acceleration seismograms. This model also cannot be applied directly for estimating broad-frequency band motions, considering its effective frequency range.

In this study, we determine a source model for estimating broadband motions using a forward modeling approach by the EGF method. We assume that ground motions are generated from several asperities, each of which has a uniform stress drop with a finite extent on the mainshock fault plane and obeys an ω^{-2} spectral scaling. Their initial locations are determined based on an inverted slip model. From the initial model, we find the best model in the sense of the fit of synthesized motions to the observed motions using a forward trial-and-error approach. Finally, using the best source model, we simulate the strong ground motions in the heavily damaged area of Kobe city.

Empirical Green's Function Method

Since Hartzell's pioneering study (1978), the semi-empirical method for synthesizing ground motions from a large earthquake by using actual small-event motions as the Green's functions instead of the theoretical Green's function has been developed by many researchers (e.g., Irikura, 1986; Dan *et al.*, 1989; Ikeura and Takemura, 1990). Moreover, the idea of the EGF method was extensively applied for in-

verting for the rupture process in source areas (Fukuyama and Irikura, 1986). Irikura (1986) formulated the EGF method to match the scaling of source spectra as well as the scaling of source parameters, in which both large and small events follow the ω^{-2} model. The ground motions from a large event are expressed as a superposition of the records of small events as follows:

$$U(t) = C \sum_{i=1}^N \sum_{j=1}^N \frac{r}{r_{ij}} F(t - t_{ij}) * u(t), \quad (1)$$

where

$$t_{ij} = \frac{r_{ij} - r_0}{\beta} + \frac{\xi_{ij}}{V_R} \quad (2)$$

$$F(t) = \delta(t) + \frac{1}{n'} \sum_{k=1}^{(N-1)n'} \delta \left[t - (k-1) \frac{\tau}{(N-1)n'} \right], \quad (3)$$

and $U(t)$ and $u(t)$ are the ground motion for a large event and the observed record of a small event used as the EGF, respectively. The terms r , r_{ij} , and r_0 are the respective distances from the site to the hypocenter of a small event, from the site to the (i, j) subfault, and from the site to the starting point of rupture on the fault plane of the large event. The term ξ_{ij} is the distance between the starting point and (i, j) subfault, β is the shear wave velocity, V_R is the rupture velocity, τ is the rise time of the large event, C is the stress-drop ratio for the large and small events, and n' is an arbitrary integer number to shift the artificial periodicity to a frequency higher than that of interest. The scaling parameter N is obtained from equation (4):

$$N = \left(\frac{M_{0r}}{CM_{0s}} \right)^{1/3}, \quad (4)$$

where, M_{0r} and M_{0s} are the seismic moments for the large and small events, respectively.

This formulation can be easily extended to cases where the target event consists of multiple shocks, each of which follows the ω^{-2} model. The omega-squared model used here means that the source displacement spectrum has a flat level at low frequencies and an omega-squared decay at high frequencies beyond a corner frequency but not always a constant stress drop between large and small events.

In this study, we use this formulation to estimate a source model of the 1995 Hyogo-ken Nanbu earthquake by forward modeling. The inverted source models as shown later have some separate regions with relatively large moment releases, so-called asperities. In simulating ground motions from the mainshock, we assumed that the ground motions are generated only from the asperities, each of which has a uniform stress drop in a finite extent on the mainshock fault plane. In other words, we synthesize mainshock ground motions based on the assumption that the mainshock consists

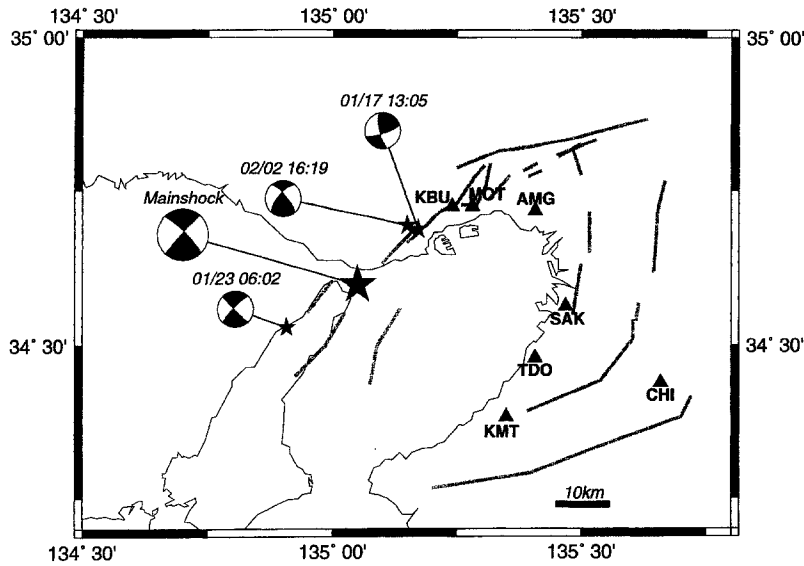


Figure 1. Map showing the station locations and epicenters of the mainshock (large star) and the aftershocks (small stars) that are used as the empirical Green's functions. The fault mechanism of the mainshock is determined using the initial motion.

of multiple events, which are located in the respective asperities.

Strong-Motion Data

In our simulation, we used velocity strong motions at six stations obtained by the Committee of Earthquake Observation and Research in the Kansai Area (CEORCA) and one from the Research Reactor Institute, Kyoto University. The locations of these stations are shown in Figure 1 together with the epicenters of the mainshock and the aftershocks used here as empirical Green's functions. Table 1 gives the station abbreviations and locations as well as the site geology. Table 2 shows the locations and the magnitudes of the aftershocks. The original velocity seismograms at MOT and AMG were clipped in amplitude larger than 40 cm/sec. Therefore, we used the restored seismograms based on the saturation characteristics of the sensor (Kagawa *et al.*, 1996). The restored records are available for velocity and displacement, but not for acceleration, because the differentiation of the restored records is less reliable.

First, we estimate the source parameters of the aftershocks. Here, we estimate the seismic moment (M_0) from the flat level (Ω_0) in the low-frequency range of the displacement source spectra, expressed by equation (5), and the corner frequency (f_c) from the intersection of both asymptotes in the low- and high-frequency ranges.

$$M_0 = \frac{4\pi\rho R\beta^3\Omega_0}{R_{\theta\phi}}, \quad (5)$$

where ρ , R , β , and $R_{\theta\phi}$ are density, hypocentral distance, S-wave velocity, and radiation coefficient, respectively; $R_{\theta\phi}$ is taken as 0.63 as the average value (Boore and Boatwright, 1984). The displacement spectrum is computed as vectorial summation of two horizontal components that were recorded

Table 1
Locations of Strong-Ground-Motion Stations

Station Name	Latitude (deg)	Longitude (deg)	Soil
KBU	34.725	135.240	rock
MOT	34.725	135.281	diluvium
AMG	34.718	135.408	alluvium
SAK	34.564	135.469	alluvium
TDO	34.480	135.408	diluvium
KMT	34.382	135.354	diluvium
CHI	34.439	135.659	rock
KMC	34.730	135.286	rock
FKI	34.718	135.281	alluvium
ASY	34.724	135.309	alluvium

Table 2
Empirical Green's Functions

Date	Latitude (deg)	Longitude (deg)	Depth (km)	Magnitude (JMA)
Aftershock 1 1995/01/17 13:05	34.688	135.172	15.0	4.7
Aftershock 2 1995/02/02 16:19	34.695	135.150	17.9	4.2
Aftershock 3 1995/01/23 06:02	34.530	134.907	15.0	4.5

at rock site. Since the resultant M_0 is estimated as an average of calculations at several sites, the effects of radiation pattern are expected to be smoothed out to some extent. Then, we confirmed that the displacement source spectra of the aftershocks used here almost follow the ω^{-2} spectral model. Another important parameter, static stress drop ($\Delta\sigma$), is estimated from the seismic moment (M_0) and the fault size (r) obtained from the corner frequency using the Brune's model (1970, 1971),

$$\Delta\sigma = \frac{7}{16} \frac{M_0}{r^3}. \quad (6)$$

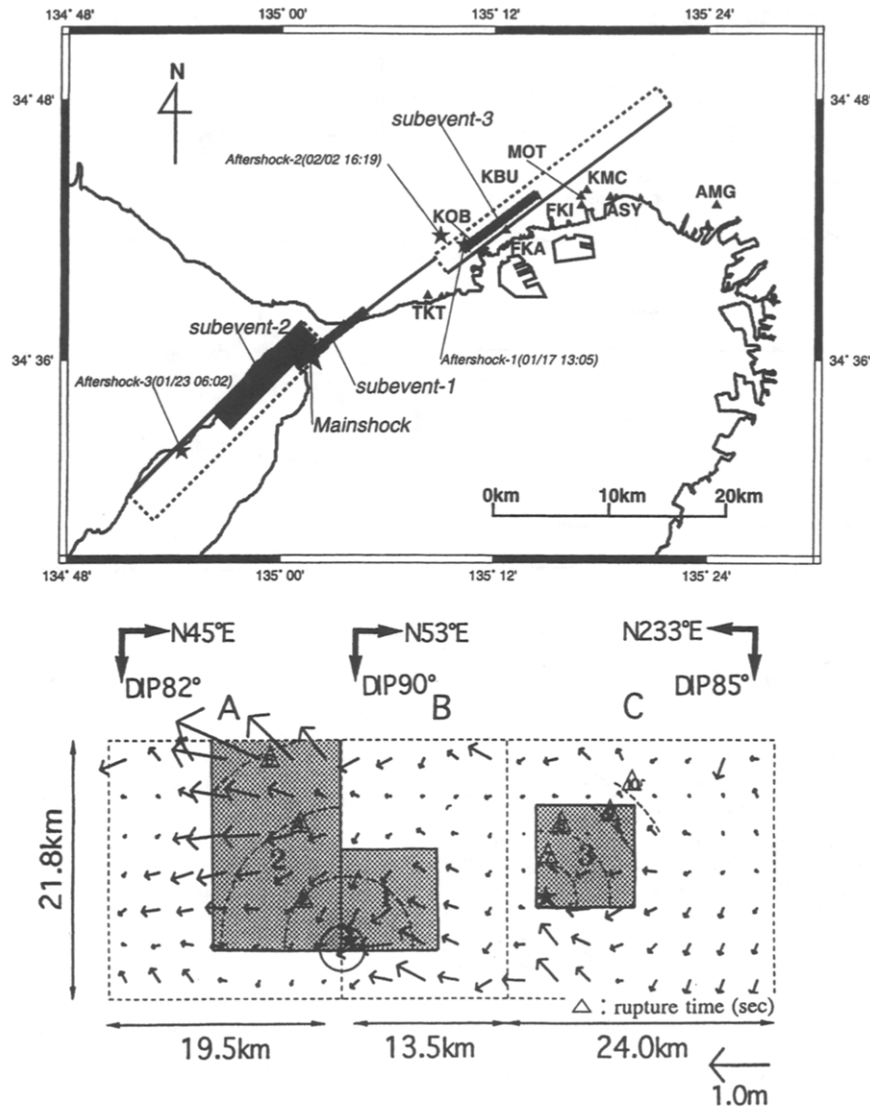


Figure 2. Source model consisting of three asperities estimated from forward modeling using the empirical Green's function method. Our model (hachured) is superimposed on the model of Sekiguchi *et al.* (1996). Source parameters for each subevent are summarized in Table 4. We assumed that ground motions are generated only from the hachured zone in the fault plane. Respective number of subfaults (N) and stress-drop ratio (C) for subevent 1 in case of using aftershocks 1 and 2 are 5 and 3.6, 10 and 1.9; for subevent 2 in case of using aftershocks 1 and 3, are 9 and 1.9, 12 and 1.1; for subevent 3 in case of using aftershocks 1 and 2 are 5 and 1.9, 10 and 1.0.

The source parameters for three aftershocks are summarized in Table 3. Furthermore, we confirmed that the fault mechanisms of three aftershocks are similar to that of the mainshock as shown in Figure 1 (Nakagawa and Iwata, 1997).

Source Model and Synthetics

Several researchers have determined the rupture model of the 1995 Hyogo-ken Nanbu earthquake from the inversion of strong-ground-motion records, some including other

Table 3
Source Parameters for Aftershocks

	M_0 (N*m)	f_c (Hz)	S (km ²)	$\Delta\sigma$ (bars)	M_{TMA}
Aftershock 1	7.1×10^{15}	1.5	2.4	46	4.7
Aftershock 2	1.7×10^{15}	3.2	0.6	86	4.2
Aftershock 3	4.5×10^{15}	2.1	1.2	82	4.5

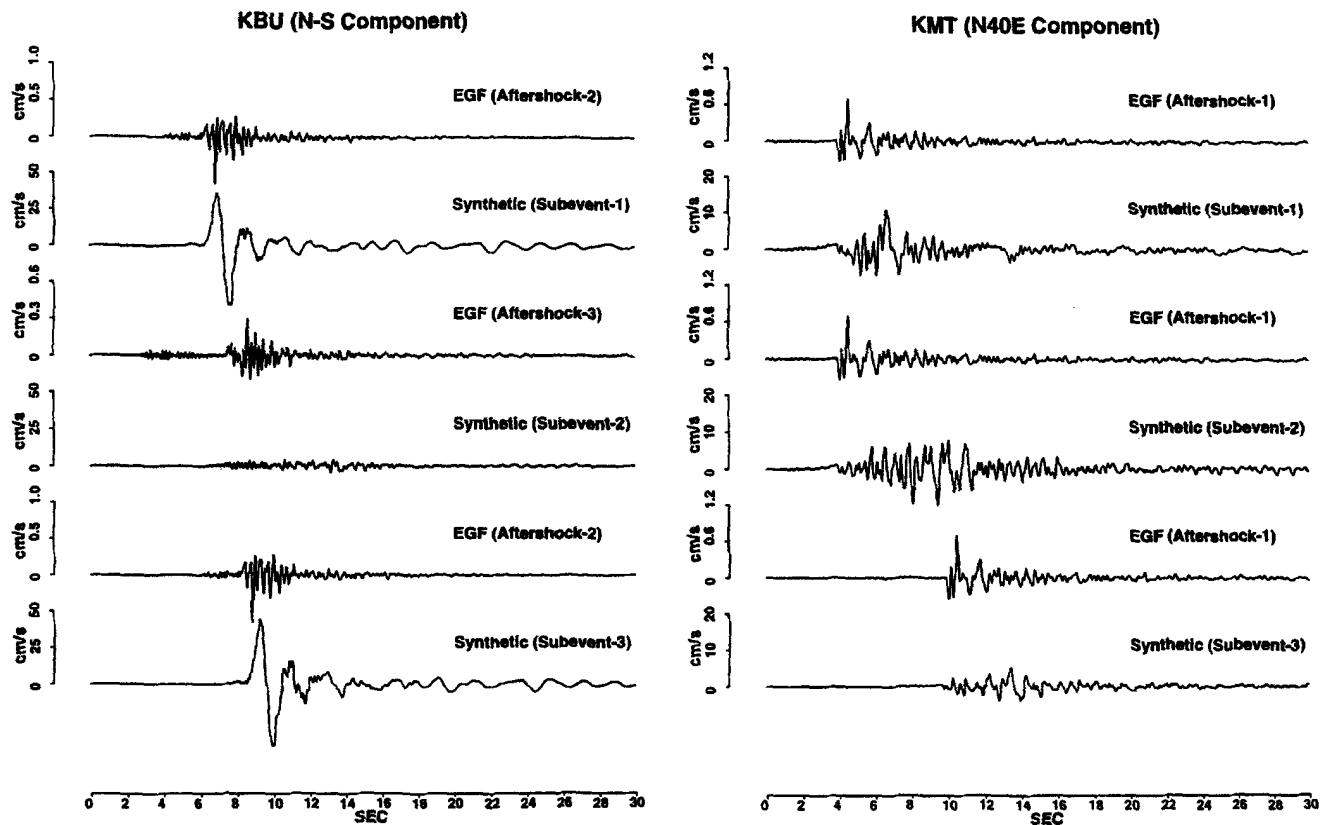


Figure 3. Separate contributions of subevents 1, 2, and 3 to the synthetics at KBU and KMT. Aftershock data used as EGF for each subevent are depicted above each synthetic.

Table 4
Source Parameters for Three Subevents

	M_0 (N^*m)	L (km) \times W (km)	$\Delta\sigma$ (bars)	Depth of Top (km)
Subevent 1	3.4×10^{18}	8×8	163	8
Subevent 2	1.0×10^{19}	11×16	86	0
Subevent 3	1.8×10^{18}	8×8	86	5

information (e.g., Sekiguchi *et al.*, 1996; Wald, 1996; Yoshida *et al.*, 1996; Ide and Takeo, 1996). On the other hand, Kakehi *et al.* (1996) estimated the radiation process of high-frequency seismic waves by the envelope inversion of acceleration seismograms between 2 and 10 Hz. The general features of those models are very similar to each other. These inverted source models have three separate regions with relatively large moment release, hereafter referred to as asperities. The first asperity is located near the rupture nucleation point under the Akashi Strait; the second, in the shallow part of the Nojima Fault in Awaji Island; and the third, under downtown Kobe city. Comparing those models in detail, however, we can see that there are some differences in the location of the third asperity. Hartzell *et al.* (1996) have also presented that the sites of low-frequency asperities are not always consistent with the regions of significant high-fre-

quency radiation from the waveform and envelope inversions for the 1994 Northridge earthquake. The total slip vector distribution obtained by Sekiguchi *et al.* (1996) is shown in Figure 2. The horizontal extent of the ruptured area is about 45 km, from 15 km southwest of the epicenter to 30 km northeast of the epicenter, and the vertical extent is from near-surface down to about 20 km. One of our objectives in this study is to determine a source model capable of explaining broadband motions containing low- and high-frequency components. To accomplish this, first, we assume a simplified source model for the initial model, considering the inverted rupture process based roughly on the Sekiguchi *et al.* (1996) model, because they carefully located the fault segments from the investigation of particle motion diagrams observed in the near-source region. Next, we adjust the locations, sizes, and stress parameters of those three asperities to fit the simulated motions to the observed using a forward modeling approach. We assumed that the ground motions are generated only from the three asperities that correspond to subevent 1 under Akashi Strait, subevent 2 along the Nojima Fault, and subevent 3 under Kobe, respectively.

We assumed an S -wave velocity of 3.5 km/sec along the wave propagation path and a rupture velocity of 2.8 km/sec on the fault plane. The rupture started from the hypocenter under the Akashi Strait and propagated to both Kobe and

Awaji Island. The rupture of subevent 3 located under Kobe city starts from the southwest bottom after the rupture reaches that point. We adopted the rise time of 0.6 sec for each subevent using a trial-and-error approach.

We used the aftershock records bandpass filtered between 0.2 and 20 Hz, depending on the signal-to-noise ratios, as the empirical Green's functions. Near-source ground motions from the mainshock at three stations, KBU, MOT, and AMG, were synthesized using two aftershock records (aftershocks 2 and 3) to represent paths from each subevent to the receivers. The motions from subevents 1 and 3 are synthesized from the records of aftershock 2 occurring between subevents 1 and 3. Those from subevent 2 are done from aftershock 3 occurring in the Awaji Island. Ground motions at stations, SAK, TDO, KMT, and CHI, several tens of kilometers away from the source, are synthesized using the records of only one aftershock (aftershock 1) occurring around a middle point of the entire mainshock fault plane. From our experience (e.g., Irikura and Kamae, 1994), the simulation event using one aftershock record is feasible for a long distance site because the propagation path effects from any point on the fault plane to the site are not significantly different compared with those for a near-source site. Frankel (1995) also successfully simulated the mainshock ground motions during the Loma Prieta earthquake using only one aftershock data.

After several trials, we obtained the best source model (Fig. 2). The source parameters for each subevent are summarized in Table 4. Here, the sizes and stress drops for subevents 1 and 3 were determined to match the predominant period and velocity amplitude of two large pulses seen at KBU and MOT. For subevent 2, these parameters were determined from the comparison between the synthesized and the observed at KMT and CHI. As presented later, the contribution of subevent 2 to the waveforms at KBU and MOT is negligible. In contrast, the waveforms at KMT, CHI, SAK, and TDO, far away from the source area, are strongly influenced by the contribution from subevent 2. Subevent 3 plays an important role of forming near-source ground motions in Kobe. The location of the asperity corresponding to subevent 3 is slightly different between the inverted source models as mentioned before. Therefore, we determine the location and stress drop of subevent 3 by fitting the synthesized motions to the observed ones at KBU and MOT. The location of subevent 3 in our best model is shallower than the part of relatively large slip under Kobe inverted by Sekiguchi *et al.* (1996), as shown in Figure 2. Our location of subevent 3 matches well the slip distribution in the Kobe side by Yoshida *et al.* (1996). The inverted source model recently retried by Irikura *et al.* (1996) using additional strong-motion data showed that large slips corresponding to subevent 3 appeared shallower than those by Sekiguchi *et al.* (1996). Furthermore, we assumed a rupture delay of 0.5 sec after the rupture reaches to the asperity of subevent 3 and before it starts to break, in order to explain the time lag between the two large pulses seen at KBU.

Separate contributions of subevents 1, 2, and 3 to the synthetics at KBU and KMT are shown in Figure 3. The contributions of subevents 1 and 3 to the waveforms at KBU are very strong because of the forward rupture directivity effect in addition to the short source distance, making two large pulses. The separate contributions at MOT are almost similar to those at KBU. In contrast, the main contributions to the ground motion at KMT are from subevents 1 and 2.

Finally, the mainshock motions are obtained by the summation of respective motions generated from the three subevents. The synthesized motions at KBU, MOT, and KMT are compared with the observed ones in Figure 4. We find that the velocity and displacement synthetics at KBU and MOT, which are located close to the causative faults, show good agreement with the observed motions. The synthetics at KMT located about 45 km from the causative fault also show good agreement with the observed in terms of peak amplitude and duration, although the matching of waveforms is not as good as for KBU and MOT.

Figure 5 shows the comparison between the synthetic and observed pseudo-velocity response spectra (PVRS) for a damping factor of 0.05. The synthesized PVRS agree well with the observed ones over a broad period range for both horizontal components in almost all of the stations we analyzed. The comparison in peak velocity and acceleration is summarized in Table 5. We find that the synthesized values agree well with the observed values, suggesting that the simplified asperity model is useful for estimating ground motions at stations ranging from a few kilometers to about 50 km.

The synthetic accelerations at soft-soil sites (SAK and TDO) contain higher frequencies than the observed ones. This might be due to the nonlinear behavior of soft-soil layers that is not considered in our simulation (Aguirre and Irikura, 1995). Since the synthetic acceleration at KBU near rock site slightly overestimates the observed one, another reason might be the difference of f_{\max} between the mainshock and the aftershock. The f_{\max} of the source spectrum of the mainshock estimated from observed seismograms at rock sites, KBU and CHI, is around 4 Hz, while that of the aftershock is higher (around 10 Hz). However, we cannot emphasize the possibility of the source-dependent f_{\max} because of such a discrepancy not appearing in all sites we analyzed.

Estimation of Strong Ground Motion in the Heavily Damaged Area in Kobe

We attempt to simulate ground motions from the mainshock at the FKI, ASY, and KMC stations in Figure 6, using the EGF method based on the same source model (Fig. 2) as shown in the previous section. FKI and ASY are located in a heavily damaged area, while KMC is near rock outcrop (hereafter, we call KMC simply on rock). We have two mainshock recordings at TKT (Nakamura *et al.*, 1996) and FKA (Osaka Gas Company) located very near the damaged area

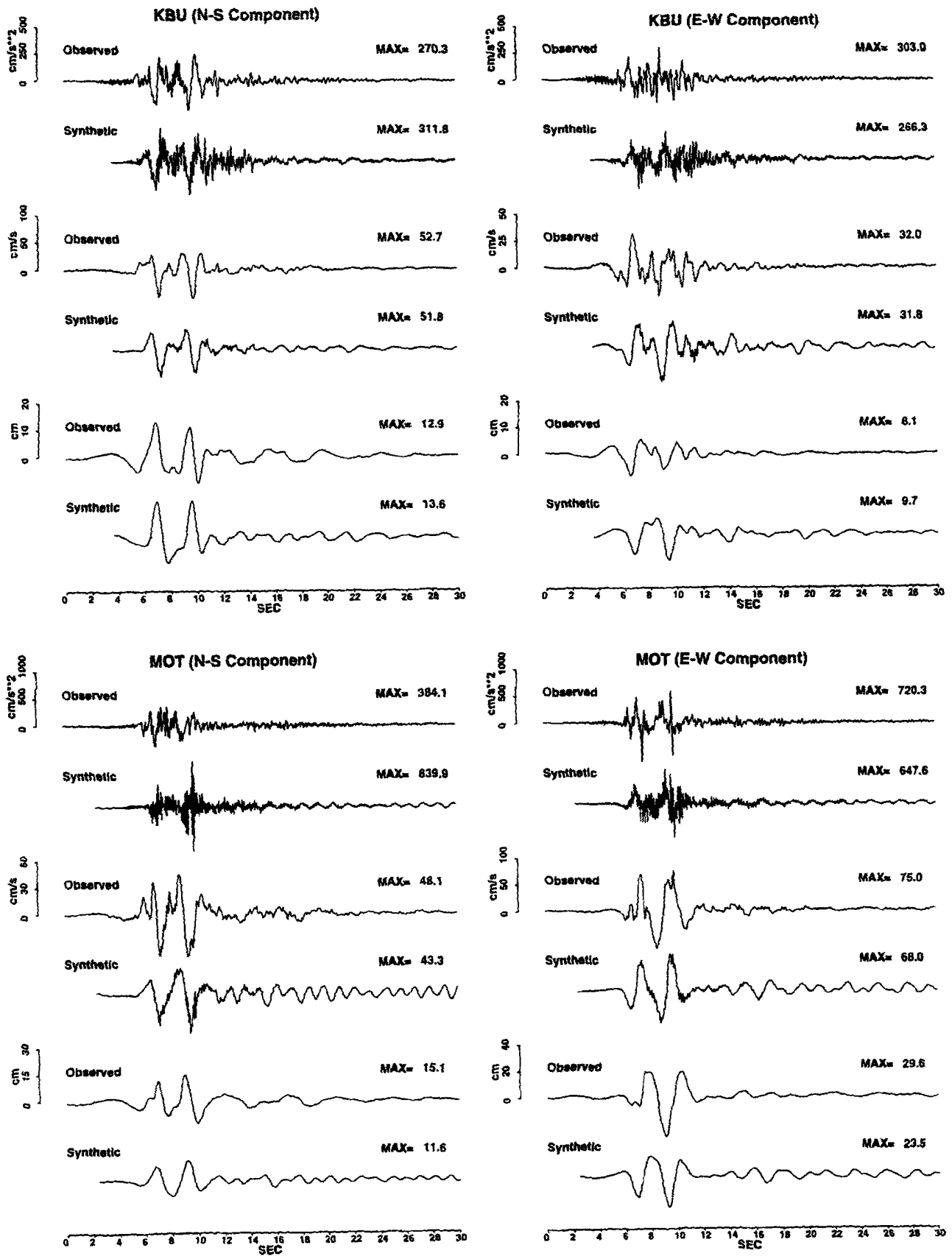


Figure 4. Comparison between the synthetics and observed motions at KBU, MOT, and KMT (continued on next page).

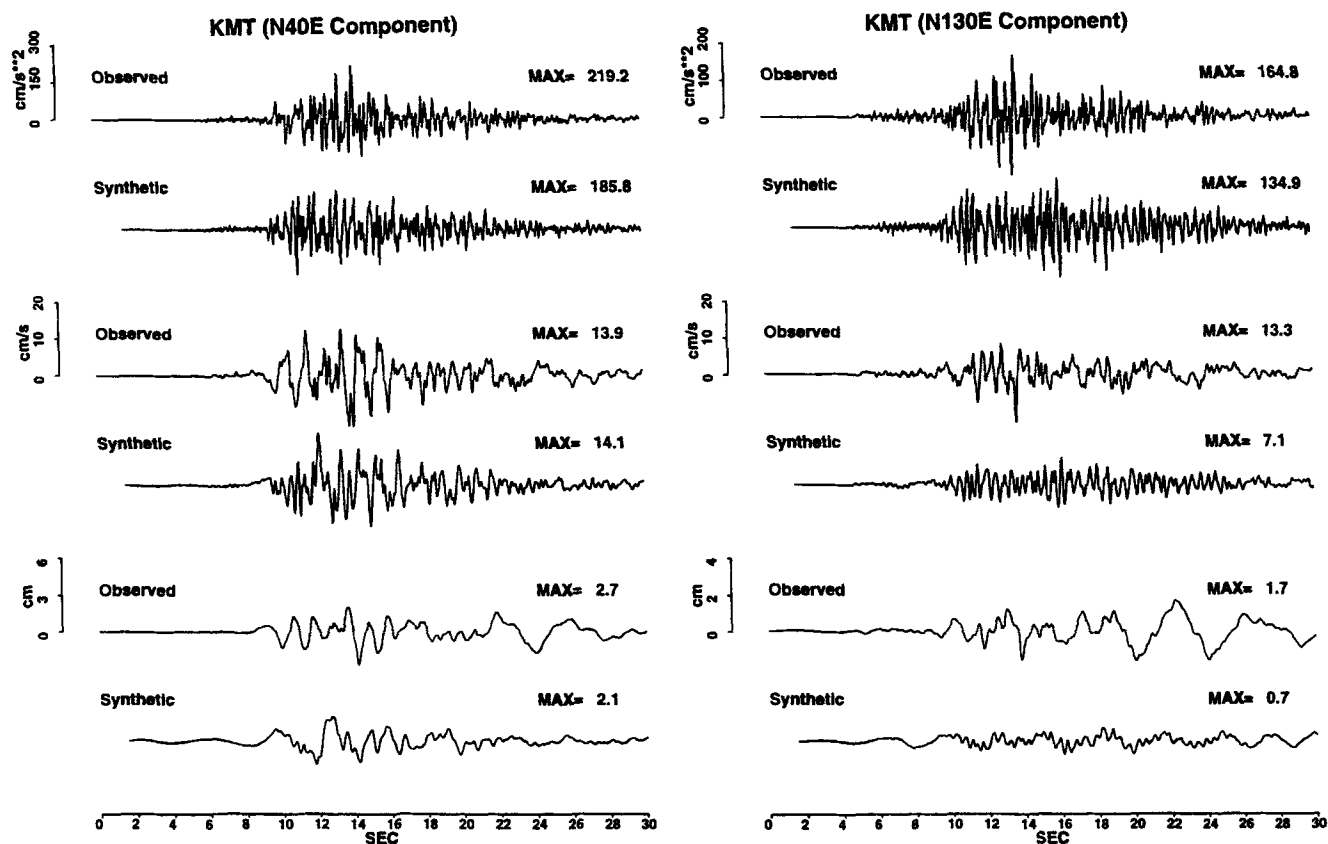


Figure 4. Continued.

(Fig. 2), although the aftershock records there were not obtained. Then we could not examine the synthesized motions with the observed ones at these two stations. Nevertheless, these data are useful in validation of our simulation in the heavily damaged area. We used only the records of aftershock 2 as the empirical Green's functions, primarily because of restrictions in the aftershock data set. We consider that the ground motions reproduced using only this aftershock are reliable because the main contributions to sites in Kobe are due to subevents 1 and 3, as shown in Figure 3. Iwata *et al.* (1995, 1996) showed that peak horizontal accelerations of this aftershock in the damaged area (FKI and ASY) were several times larger than those at KMC on rock, implying that the observed records reflect the site characteristics.

The synthesized ground motions at KMC on rock and at FKI and ASY in the heavily damaged area are shown in Figure 7. The strong ground motions synthesized here as well as those observed at KBU and MOT in the near-source area are composed of two large pulses each with a duration of 1 to 3 sec. The large pulses dominate in the horizontal component, normal to the fault plane. Similar near-source ground-motion characteristics were observed during the 1994 Northridge earthquake and the 1989 Loma Prieta earthquake, even though these earthquakes had different faulting mechanisms. These pulses are indicative of the forward rup-

ture directivity focusing on near-source ground motion (Heaton *et al.*, 1995; Somerville *et al.*, 1995). Heaton *et al.* (1995) has warned that these ground motions would cause large deformation and possible collapse of steel-framed buildings and the base-isolated buildings.

The synthetic velocity motions at KMC are very similar to the observed ones at rock site KBU. The peak horizontal acceleration and velocity of the synthetic motions at KMC are about 300 cm/sec² and 57 cm/sec, respectively, almost the same level as those observed at KBU. In contrast, peak horizontal accelerations of the synthetic motions at FKI and ASY in the heavily damaged area are about 900 and 1000 cm/sec², respectively, a little larger than the observed ones at FKA (810 cm/sec²) and at TKT (666 cm/sec²). The peak horizontal velocities of the synthetic motions at FKI and ASY are about 130 and 115 cm/sec, respectively, comparable to those observed at FKA (121 cm/sec) and at TKT (138 cm/sec).

Kawase *et al.* (1995) has reproduced ground motions for the same sites in the heavily damaged area using equivalent linear or effective stress analysis with soil models that were derived from aftershock records. They used the mainshock record at KBU as an input motion to the base rock and concluded that the ground motions in the heavily damaged area must have reached at least the level of 600 cm/sec² in acceleration and 130 cm/sec in velocity. Their results seem

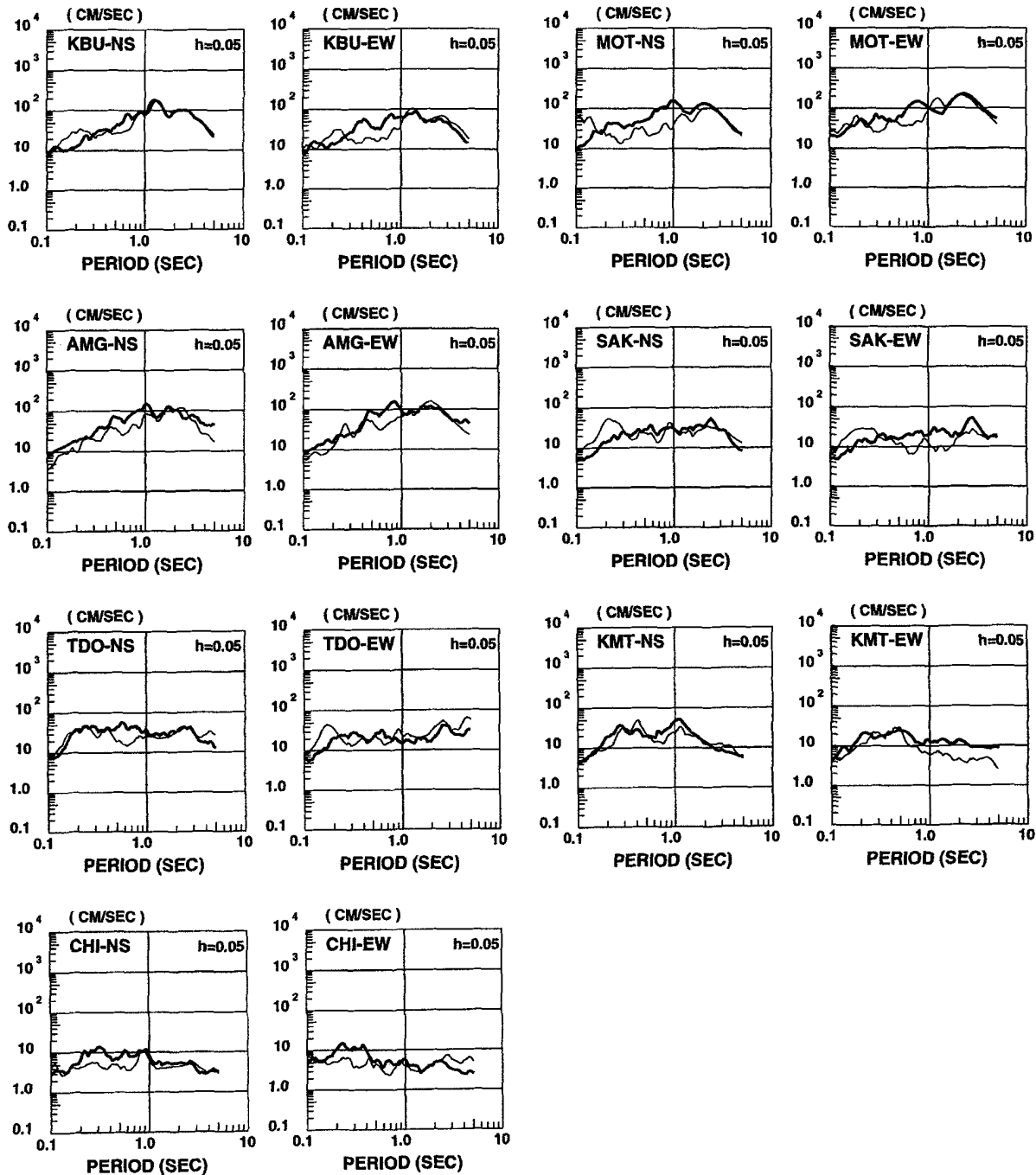


Figure 5. Comparison of the pseudo-velocity response spectra (PVRS) with damping factor of 0.05 of the synthesized motions and those of the observed motions. Solid thin line shows the PVRS of the synthesized motions. Solid thick line shows the PVRS of the observed motions.

to be consistent with our results in peak velocity amplitudes, although they estimate smaller peak acceleration because of the nonlinear effects.

Figure 8 shows the pseudo-velocity response spectra of the synthetic ground motions in the heavily damaged area, plotted with a number of observed spectra. The spectra with larger amplitude in two horizontal components are shown in

this figure. The response spectra at periods of 1 to 3 sec at FKI, ASY (the reproduced) and TKT, FKA (the observed) are significantly larger than those at KOB (JMA station) in the less-damaged area as well as at the Tarzana station without any damages around there, in spite of its very large acceleration amplitude (about 1.8 g) during the 1994 Northridge earthquake.

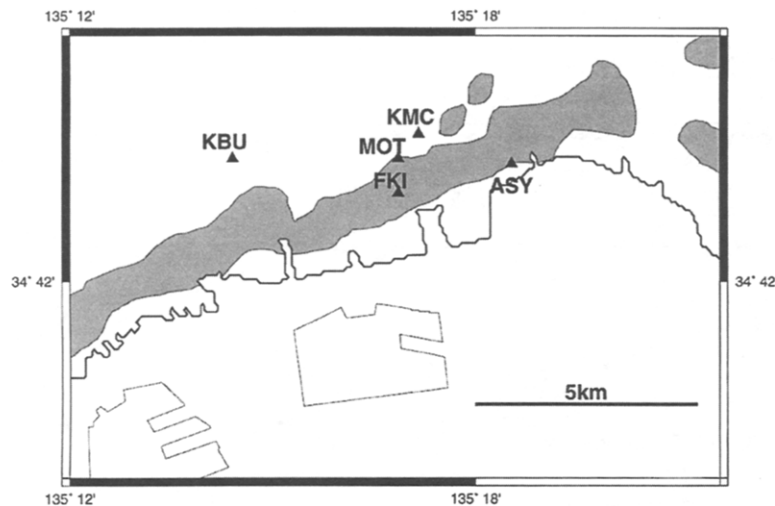


Figure 6. Location of array observation stations (KMC, FKI, and ASY) in Higashinada Ward, Kobe city. Gray zones show the heavily damaged area (JMA Intensity 7) in Kobe city (Koketsu, 1997). Solid triangles (KMC, FKI, ASY) indicate temporal stations for aftershock observation.

Table 5
Comparison of Peak Amplitudes of the Synthesized Motions
and Those of the Observed Ones

Station	Observed				Synthetic				Synthetic/Observed			
	Acceleration (cm/sec ²)		Velocity (cm/sec)		Acceleration (cm/sec ²)		Velocity (cm/sec)		Acceleration (cm/sec ²)		Velocity (cm/sec)	
	N-S	E-W	N-S	E-W	N-S	E-W	N-S	E-W	N-S	E-W	N-S	E-W
KBU	270.3	303.0	52.7	32.0	311.8	266.3	51.8	31.8	1.15	0.88	0.98	0.99
MOT*	—	—	48.1	75.0	839.9	647.6	43.3	68.0	—	—	0.90	0.91
AMG*	—	—	40.9	53.5	202.3	260.4	28.1	49.3	—	—	0.69	0.92
SAK	149.7	121.1	14.2	13.0	364.6	302.4	16.5	10.8	2.44	2.50	1.16	0.83
TDO	287.7	186.4	24.2	15.0	413.6	279.1	17.4	19.7	1.44	1.50	0.72	1.31
KMT	219.2	164.8	13.9	13.3	185.8	134.9	14.1	7.1	0.85	0.82	1.01	0.53
CHI	88.7	109.2	5.0	4.2	75.2	93.0	3.3	3.6	0.85	0.85	0.66	0.86

*Peak velocity amplitudes of the restored seismograms by Kagawa *et al.* (1996).

Near-source ground motions in Kobe were characterized by two large pulses due to two asperities lying under Akashi and Kobe and the forward rupture directivity. The difference in peak amplitude between the damaged sites such as FKI and ASY and less-damaged sites KOB and MOT is significantly due to the relative location from the basin edge. Pitarka *et al.* (1996, 1997) showed that the ground motion from an aftershock are largely amplified at FKI and ASY in the damaged area offset by about 1 km from the basin edge by the superposition of the direct *S* waves and the basin-edge-diffracted waves. That is, in the heavily damaged area, the large pulses due to the forward rupture directivity effects could be furthermore amplified due to the basin-edge effects and the local site effects. The large response at one to three periods may be related to the damaging effects of ground motions on buildings and bridges (Minami and Sakai, 1996).

Conclusions

To investigate why Kobe and adjacent cities were so severely devastated by the 1995 Hyogo-ken Nanbu earthquake, we estimated strong ground motions at heavily dam-

aged sites in Kobe city where the mainshock was not recorded, using aftershock records. First, we confirmed that the source model consisting of three asperities on the fault plane is valid to explain the main features of the observed near-source ground motions by comparing synthetic and observed seismograms. We found that the synthetic near-source ground motions in Kobe were characterized by two large pulses caused by the forward rupture directivity of two asperities lying under Akashi and Kobe. The peak horizontal acceleration and velocity of the simulated ground motions at the heavily damaged sites are about 1,000 cm/sec² and 130 cm/sec, respectively, while those at a rock site in the near-source area (less than 1 km from the fault) are about 300 cm/sec² and 60 cm/sec, almost the same level recorded at KBU. We conclude that the large response amplitudes around 1 to 3 sec caused the heavy damage to buildings and bridges.

Acknowledgments

We thank the Committee of Earthquake Observation and Research in the Kansai Area for providing us with the velocity records, and Mr. Takao

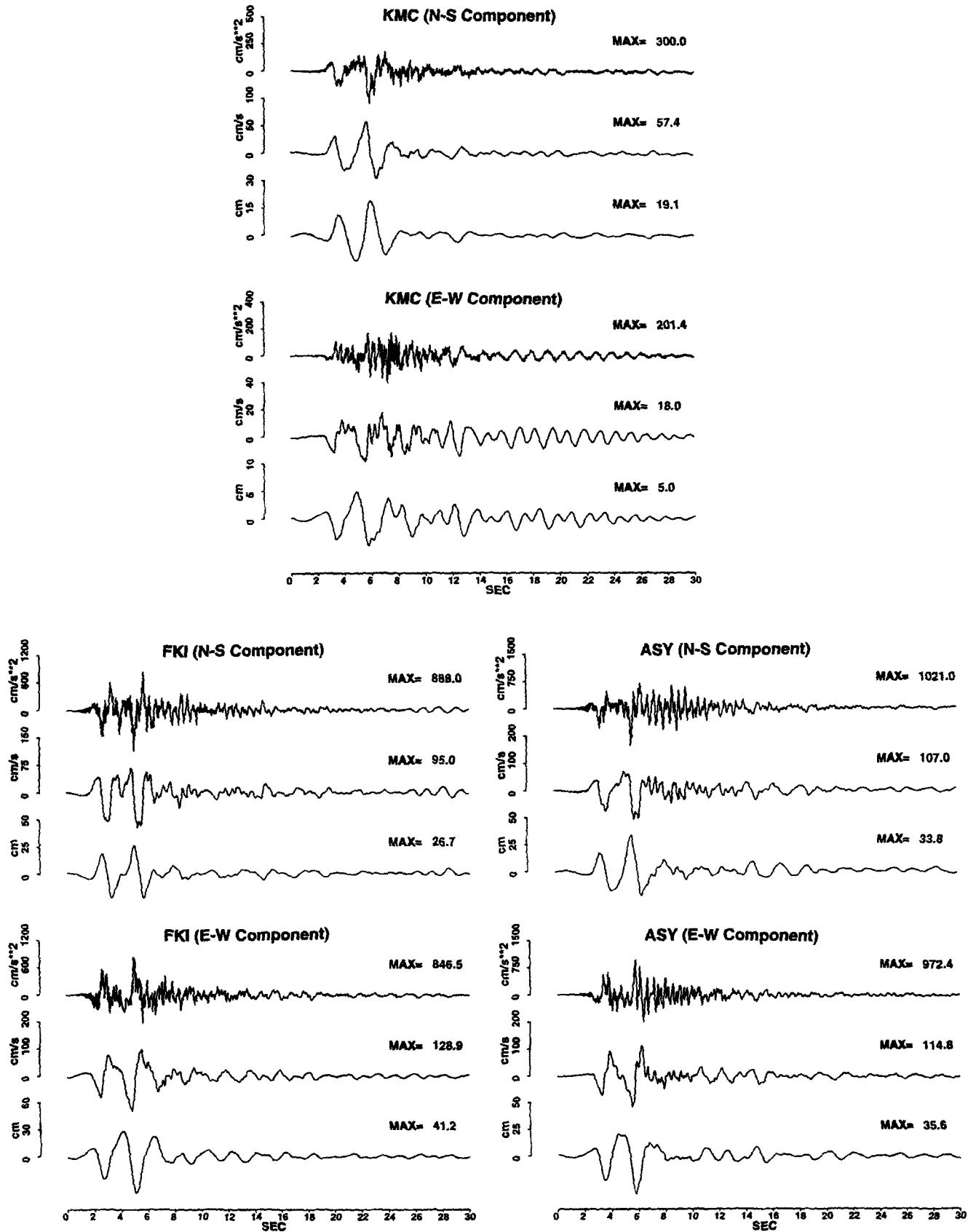


Figure 7. Synthesized ground motions (acceleration, velocity, and displacement) at KMC near rock, FKI, and ASY in the heavily damaged area.

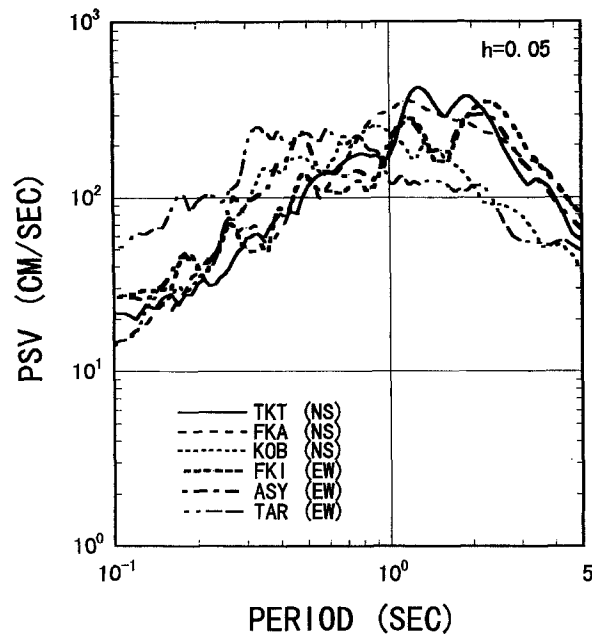


Figure 8. Comparison of the PVRs with damping factor of 0.05 of the synthesized motions in horizontal E-W component at FK1 and ASY in the heavily damaged area as well as the observed at TKT and FKA in the near-heavily damaged area, and those of the observed motions at the less damaged site KOB as well as at Tarzana station during the 1994 Northridge earthquake.

Kagawa for the restored velocity record at MOT and AMG stations. We would like to thank the Railway Technical Research Institute and Osaka Gas Company for providing us with the respective mainshock motion at stations TKT (Serial No. R-032) and FKA, and K. Koketsu for providing us with the digitalized data for JMA Intensity 7 area. We are grateful to T. Iwata and H. Sekiguchi for their valuable discussions. We greatly appreciate the useful review by two anonymous reviewers. This study was partially supported by a Grant-In-Aide for Scientific Research, Number 08248111, from the Ministry of Education, Science, Sports, and Culture.

References

- Aguirre, J. and K. Irikura (1995). Preliminary analysis of non-linear site effects at Port island vertical array station during the 1995 Hyogo-ken Nanbu earthquake, *J. Natural Disast. Sci.* **16**, 49–58.
- Boore, D. M. and J. Boatwright (1984). Average body-wave radiation coefficient, *Bull. Seism. Soc. Am.* **72**, 1049–1068.
- Brune, J. N. (1970). Tectonic stress and the spectra of seismic shear waves from earthquake, *J. Geophys. Res.* **75**, 4997–5009.
- Brune, J. N. (1971). Correction, *J. Geophys. Res.* **76**, 5002.
- Dan, K., T. Watanabe, and T. Tanaka (1989). A semi-empirical method to synthesize earthquake ground motions based on approximate far-field shear wave displacement, *J. Struct. Constr. (Trans. AIJ)* **396**, 27–36 (in Japanese).
- Frankel, A. (1995). Simulating strong motions of large earthquakes using recordings of small earthquakes: the Loma Prieta mainshock as a test case, *Bull. Seism. Soc. Am.* **85**, 1144–1160.
- Fukuyama, E. and K. Irikura (1986). Rupture process of the 1983 Japan Sea (Akita-Oki) earthquake using a waveform inversion method, *Bull. Seism. Soc. Am.* **76**, 1623–1640.
- Hartzell, S. H. (1978). Earthquake aftershocks as Green's functions, *Geophys. Res. Lett.* **5**, 1–4.
- Hartzell, S. H., P. Liu, and C. Mendoza (1996). The 1994 Northridge, California, earthquake: investigation of rupture velocity, risetime, and high-frequency radiation, *J. Geophys. Res.* **101**, 20091–20108.
- Heaton, T. H., J. F. Hal, D. J. Wald, and M. N. Halling (1995). Response of high-rise and base-isolated buildings to hypothetical Mw 7.0 blind thrust earthquake, *Science* **267**, 206–211.
- Horikawa, H., K. Hirahara, Y. Umeda, M. Hashimoto, and F. Kusano (1996). Simultaneous inversion of geodetic and strong motion data for the source process of the Hyogo-ken Nanbu, Japan, earthquake, *J. Phys. Earth* **44**, 455–472.
- Ide, S. and M. Takeo (1996). Source process of the 1995 Kobe earthquake: determination of spatio-temporal slip distribution by bayesian modeling, *Bull. Seism. Soc. Am.* **86**, 547–566.
- Ikeura, T. and M. Takemura (1990). Scaling relation of source spectra as a basis of a semi-empirical method for synthesizing strong ground motions due to heterogeneous faulting, *Zishin, Ser. II, (J. Seism. Soc. Japan)* **43**, 483–492 (in Japanese with English abstract).
- Irikura, K. (1986). Prediction of strong acceleration motion using empirical Green's function, *Proc. 7th Japan Earthquake Symp.*, 151–156.
- Irikura, K. (1995). Causative faults, strong ground motions and damages from the 1995 Hyogo-ken Nanbu earthquake, *Butsuri-Tansa (J. Soc. Exploration Geophys. Japan)* **48**, 463–489 (in Japanese).
- Irikura, K. and K. Kamae (1994). Estimation of strong ground motion in broad-frequency band based on a seismic source scaling model and an empirical Green's function technique, *Annali di Geofisica* **37**, 1721–1743.
- Irikura, K., T. Iwata, H. Sekiguchi, A. Pitarka, and K. Kamae (1996). Lesson from the 1995 Hyogo-ken Nanbu earthquake: Why were such destructive motions generated to buildings?, *J. Natural Disast. Sci.* **18**, 99–127.
- Iwata, T., K. Hatayama, H. Kawase, K. Irikura, and K. Matsushima (1995). Array observation of aftershocks of the 1995 Hyogoken-nanbu earthquake at Higashinada ward, Kobe city, *J. Natural Disast. Sci.* **16**, 41–48.
- Iwata, T., K. Hatayama, H. Kawase, and K. Irikura (1996). Site amplification of ground motions during aftershocks of the 1995 Hyogo-ken Nanbu earthquake in severely damaged zone—Array observation of ground motions at Higashinada ward, Kobe city, Japan, *J. Phys. Earth* **44**, 553–562.
- Kagawa, T., K. Irikura, and I. Yokoi (1996). Restoring clipped records of near-field strong ground motion during the 1995 Hyogo-ken Nanbu (Kobe), Japan earthquake, *J. Natural Disast. Sci.* **18**, 43–57.
- Takehi, Y., K. Irikura, and M. Hoshihara (1996). Estimation of high-frequency wave radiation area on the fault plane of the 1995 Hyogo-ken Nanbu earthquake by the envelope inversion of acceleration seismograms, *J. Phys. Earth* **44**, 505–517.
- Kawase, H. (1996). The cause of the damage belt in Kobe: "The basin edge effect," constructive interference of the direct S wave with the basin-induced diffracted/rayleigh waves, *Seism. Res. Lett.* **67**, 25–34.
- Kawase, H., T. Satoh, S. Matsushima, and K. Irikura (1995). Ground motion estimation in the Higashinada ward in Kobe during the Hyogo-ken Nanbu earthquake of 1995 based on aftershock records, *J. Struct. Constr. Eng. (Trans. AIJ)* **476**, 103–112 (in Japanese).
- Kikuchi, M. (1995). Source process of the Kobe earthquake of January 17, 1995. *Chishitsu News* **486**, 12–15 (in Japanese).
- Koketsu, K. (1997). Source process of the mainshock, Joint Report on Great Hanshin-Awaji Earthquake Disaster. Vol. 1, Chap. 4, Source process, SSI, JSCE, AIJ, JGC and JSME, in print.
- Minami, T. and Y. Sakai (1996). Extremely large potential destructiveness of the ground motions measured in the 1995 Kobe earthquake in Japan, *Proc. 11th WCEE*.
- Nakagawa, H. and T. Iwata (1997). Source parameters of aftershocks of the 1995 Hyogo-ken Nanbu earthquake (3: those regionality and relation to the stress drops), Abstracts of 1997 Joint Earth and Planetary Science Joint Meeting, W12–P04.

- Nakamura, Y., F. Uehara, and H. Inoue (1996). Waveform and its analysis of the 1995 Hyogo-Ken-Nanbu earthquake (II), JR Earthquake Information No. 23d, Railway Technical Research Institute (in Japanese).
- Pitarka, A., K. Irikura, T. Iwata, and T. Kagawa (1996). Basin structure effects in the Kobe area inferred from the modeling of ground motions from two aftershocks of the January 17, 1995 Hyogoken-nanbu earthquake, *J. Phys. Earth* **44**, 563–576.
- Pitarka, A., K. Irikura, and T. Iwata (1997). Modelling of ground motion in the Higashinada (Kobe) area for an aftershock of the 1995 January, 17 Hyogo-ken Nanbu earthquake, *Geophys. J. Int.* **131**, 231–239.
- Pitarka, A., K. Irikura, T. Iwata, and H. Sekiguchi (1998). Three-dimensional simulation of the near-fault ground motion for the 1995 Hyogoken Nanbu (Kobe), Japan, earthquake, *Bull. Seism. Soc. Am.* **87**, 428–440.
- Sekiguchi, H., K. Irikura, T. Iwata, Y. Takehi, and M. Hoshihara (1996). Minute locating of faulting beneath Kobe and the waveform inversion of the source process during the 1995 Hyogo-ken Nanbu, Japan, earthquake using strong ground motion records, *J. Phys. Earth* **44**, 473–488.
- Shimamoto, T. (1995). Mystery of “Damage belt” during Kobe earthquake, *Iwanami-Kagaku (Iwanami-Science)* **65**, 195–198.
- Somerville, P. G., N. F. Smith, R. W. Graves, and N. A. Abrahamson (1995). Accounting for near-fault rupture directivity effects in the development of design ground motion, *Proc. of the 1995 ASME/JSME PVP Conference*, Hawaii, 23–27 July.
- Wald, D. J. (1996). Slip history of the 1995 Kobe, Japan, earthquake determined from strong motion, teleseismic, and geodetic data, *J. Phys. Earth* **44**, 489–504.
- Watanabe, M. and Y. Suzuki (1995). Late Quaternary activity of active faults in Kobe area, Programme and Abstracts. The Seismological Society of Japan, 2, A85 (in Japanese).
- Yoshida, S., K. Koketsu, B. Shibasaki, T. Sagita, T. Kato, and Y. Yoshida (1996). Joint inversion of near- and far-field waveforms and geodetic data for the rupture process of the 1995 Kobe earthquake, *J. Phys. Earth* **44**, 437–454.

Research Reactor Institute
 Kyoto University
 Noda, Kumatori-cho
 Sennan-gun, Osaka, 590-04, Japan
 Tel: +81-724-51-2369; Fax: +81-724-51-2603;
 E-mail: kamae@kuca.rii.kyoto-u.ac.jp
 (K.K.)

D.P.R.I.
 Kyoto University
 Gokasho, Uji
 Kyoto, 611, Japan
 Tel/Fax: +81-774-33-5866;
 E-mail: irikura@egmdpri01.dpri.kyoto-u.ac.jp
 (K.I.)

Manuscript received 28 May 1997.